

Origami-inspired foldable sound barrier designs

Xiang Yu¹⁾, Hongbin Fang²⁾, Fangsen Cui¹⁾, Li Cheng²⁾, and Zhenbo Lu³⁾*

- 1) Institute of High Performance Computing, A*STAR, Singapore, 138632
 - 2) Department of Mechanical Engineering, The Hong Kong Polytechnic University, Hong Kong, China, 999077
 - 3) Temasek Laboratories, National University of Singapore, Singapore, 117411
- *tslluz@nus.edu.sg

Abstract

Conventional sound barriers are constrained by fixed geometry which results in many limitations. In this research, *origami*, the paper folding technique, is exploited as a platform to design deployable and reconfigurable sound barriers, as well as to actively tailor the attenuation performance. As a proof of concept, a three-dimensional barrier structure is constructed based upon Miura-ori unit cells, whose shape can be significantly altered via folding with a single degree of freedom. Folding also generates periodic corrugations on the origami sheets, which can be exploited as backing cavities to form resonant sound absorbers with a micro-perforated membrane. The absorption performance of the constructed absorber and the insertion loss of the origami barrier are investigated using both numerical and experimental tools. The proposed origami barrier involves two fundamental mechanisms: sound reflection and absorption, and the origami offers unique tunability to enrich both mechanisms owing to the folding-induced geometric evolutions. Specifically, the sound reflection effect can be effectively tuned via changing the acoustic shadow zone and the diffracted sound paths by folding, and the sound absorption effect can also be regulated by altering the depth/shape of the backing cavities during folding. Overall, the results of this research offer fundamental insights into how folding would affect the acoustic performance and open up new opportunities for designing innovative origami-inspired acoustic devices.

Keywords: sound barrier, origami structure, shape-morphing, micro-perforated membrane, insertion loss.

1. Introduction

Noise barriers are widely used as effective control measures to mitigate traffic, construction, and industrial noises. The common perception of noise barriers is that they often constitute large and heavy structures, which call for considerable economic investment and impose negative visual impacts on the residents. Thus, such practices generally apply to stationary noise sources which need continuous shielding. However, in reality, some noise control requirements are temporal, for example, to reduce noise during urgent night works, occasional repair works, and refurbishments on occupied buildings. In these scenarios, constructing a permanent barrier becomes unnecessary and uneconomical; rather, a portable, reusable, and reconfigurable barrier would be attractive to accommodate various noise environments. To overcome the difficulties of conventional sound barriers and to achieve the abovementioned promises, one would require a noise barrier to be effective in controlling noise, easily transportable, simple and fast deployable, on-site reconfigurable, and relatively low-cost.

The performance of a noise barrier depends on many factors including shape, curvature, source directivity, ground impedance, and absorption treatment, etc. [1-5]. The basic function of a noise barrier is to provide geometric shielding effect by intercepting the line-of-sight between the source and receiver. Owing to this, the barrier height and the relative position of source and receiver to the barrier are the primary factors determining the sound attenuation performance. Generally, a higher barrier provides better protection over a larger area, at the expenses of incurring higher manufacturing and installation costs, which therefore calls for a design trade-

off. Many studies have attempted to alter barrier configurations without significantly increasing barrier height, such as introducing inclined/curved tops [4] and irregularly-shaped tips [3], and using topology optimization [6], but discussions were still confined to the context of fixed barriers. Apart from rigid noise barriers which are reflective, some studies have demonstrated that adding absorption could further benefit noise reduction effects. Commercial noise barrier products usually contain backs of absorbent materials such as mineral wool or metal foam, which are covered by perforated panels to form solid structures to prevent dust accumulation. As an easy way to retrofit the existing reflective barriers, modular forms of sound absorbers can be incorporated [5]. To induce minimal visual impact, transparent micro-perforated panel absorber can be employed to provide both excellent acoustic performance and visual presentation [7]. It is also possible to optimize the geometry and absorption simultaneously by using topological optimization [8]. With these efforts, significant progress has been achieved in barrier performance and appearance. Despite these efforts, new innovations are desperately needed to fundamentally advance the design philosophy of acoustic barriers so that the long-expected features can become a reality, including design flexibility and versatility, on-site and on-demand tunability, simple and fast deployment, portability and reusability, all of which are challenging objectives with the conventional techniques.

In recent years, noise barriers with novel features have been reported, such as incorporating active noise control [9], sonic crystal [10], edge geometry modification [11] and wave trapping barrier [1], most of which are based on modifying the existing

flat barrier to enhance the sound attenuation. While improving the noise control performance, these designs are still constrained by the large size, and therefore still lack adequate portability and adaptability. On the other hand, the current “mobile” sound barriers on the market actually are assemblies of soundproof panels; although detachable, they cannot be reconfigured with respect to different noise sources, and they require cumbersome human works for assembling and disassembling [12]. In sum, the fundamental question of how to design barriers which can meet the requirement for shielding temporary noises, demand less building and installation cost, possess good portability and reusability, and provide on-demand reconfigurability is still unsolved.

Recently, the ancient art of paper folding, known as *origami*, has emerged as a novel approach for achieving reconfigurable and deployable engineering applications due to the vast design possibilities and excellent folding-induced reconfigurability that it can offer. Since origami folding and the associated properties are entirely determined by the geometry that is scale-independent, origami triggers an explosion of innovations in programmable materials, structures, and devices [13-17]. The origami reconfigurability also offers great potentials in designing completely new acoustic devices, but so far, the principle has only been applied to a few examples. Based on the Miura-ori and star-shaped origami, reconfigurable acoustic arrays have been designed to reversibly control wave energy focusing [18, 19]. Inspired by modular origami techniques, three-dimensional networks of tubes are exploited to design reconfigurable origami waveguides that are capable of controlling and

redirecting the acoustic transmission and radiation pattern [20]. Origami could also be treated as a platform to guide the reconfiguration of the associated arrays of inclusions via folding, which can be potentially developed into a tunable traffic noise barrier [21, 22]. These successful applications of folding algorithms in acoustics suggest that origami could also become a novel and viable tool for designing next-generation sound barriers with unique features.

This study aims at providing a preliminary study on the mechanism and feasibility of a three-dimensional origami-inspired sound barrier. The strategy here is to use rigid plates and flexible hinges to form a Miura-ori sheet which is easily reconfigurable. By folding the origami sheet, the dimension and the surface profile of the barrier are changed on site, which would affect the sound attenuation performance in the shadow zone by altering the diffracted sound paths. Moreover, the folding-induced corrugations on the origami sheets can be exploited as backing cavities to form resonant sound absorbers via covering an absorptive facing, such as a micro-perforated membrane. Such design further improves the attenuation performance by incorporating the absorption mechanism, which is of vital importance to reduce the sound diffraction and reflection of a rigid barrier [5]. Noting that the Miura-ori possesses excellent flat-foldability, the designed barrier can therefore be folded into a compact structure with relatively small volume for convenient transportation. Without tedious assembling and disassembling processes, the barriers can be easily deployed to specified configurations. Comparing with the conventional sound barriers, the improvements brought by origami folding are obvious and exciting.

To predict the acoustic performance of sound barriers, i.e., the Insertion Loss (IL), various empirical, analytical, and numerical approaches have been developed (see a comprehensive review conducted by Li [23]). The earliest efforts were made from a geometry perspective, e.g., the Maekawa's empirical curve determines the diffracted sound based on a two-dimensional system [24]. His method has been extensively used in engineering applications owing to its simplicity, but the prediction accuracy is poor due to the lack of narrow-band details. For a three-dimensional barrier, sound diffractions would happen not only at the tip but also at the two edges. In such scenario, the simple geometry relation is incapable of capturing the interference effects generated by multiple diffraction paths, which therefore calls for a three-dimensional modeling approach. Dedicated to this, Terai [25] applied Helmholtz integral equation to accurately determine the IL of finite length barriers; later, with the advent of numerical approaches such as boundary element (BE) and finite element (FE) methods, more complex barrier configurations can be analyzed [26], although these approaches are generally computationally demanding. The advantage of numerical approach is its ability to cope with great geometric complexity and resolve the detailed sound field around the barrier.

This paper is organized as follows. Based on Miura-ori, Section 2 proposes the conceptual design of origami-inspired barrier, with particular focuses on their geometric reconfigurability and portability. We show that, in addition to being reflective, the barrier can be upgraded into absorptive by integrating the corrugation cavities with micro-perforated facing. To handle the complex origami geometry and

to obtain an accurate examination of barrier's performance, Section 3 uses numerical techniques to determine the absorption characteristics, which are verified by experiments to ensure their applicability in predicting barrier performance. Section 4 further details numerical results on the insertion losses of different origami barriers at different folding configurations, to uncover the involved mechanisms and demonstrate the folding-induced tunability.

2. Conceptual designs of foldable sound barriers

In this section, the geometry and folding kinematics of Miura-ori are introduced; based on which, conceptual designs of origami barrier are proposed. Particular attentions will be paid to demonstrating how origami would benefit the barrier development.

2.1 Origami geometry and kinematics

Figure 1(a) shows the geometry of a Miura-ori cell, which consists of four identical parallelogram facets (with sector angle α) connected by four creases intersecting at the center vertex ' O '. Half of a unit cell can be denoted by six vertex points ' A ', ' B ', ' C ', ' O ', ' D ', and ' E '. For simplicity, all crease lengths are assumed to be identical, i.e., $AB=BC=AD=DE=l$. Rigid folding can be assumed in this study, i.e., the four facets remain rigid during folding.

Folding of the Miura-ori cell is a one degree-of-freedom (DoF) mechanism [27], which can be described by the folding angle θ , defined as the angle between the crease AO and the horizontal plane (or between the crease OA' and the horizontal

plane) (Fig. 1(b)). Then all the other geometries of a folded cell can be determined [28]: the height of the unit cell is

$$H_{\text{cell}} = |BD| = 2l \sin \alpha \cos(\arcsin(\tan \theta / \tan \alpha)); \quad (1)$$

the length is

$$L_{\text{cell}} = |AA'| = 2l \cos \theta; \quad (2)$$

and the thickness is

$$T_{\text{cell}} = |OF| = l \sin \theta. \quad (3)$$

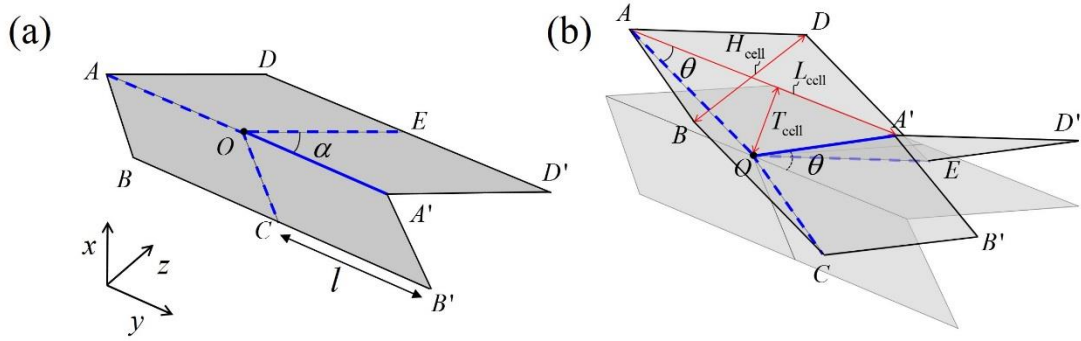


Figure 1. Geometry of a Miura-ori cell at the (a) flat state and a (b) partly folded state. The internal solid and dashed lines denote the “mountain” and “valley” creases, respectively.

2.2 Reflective barrier

By tessellating the Miura-ori cells in the horizontal y - z plane, a three-dimensional origami barrier can be constructed, as illustrated in Fig. 2(a). The external dimensions of an $M \times N$ barrier at the configuration with folding angle θ are:

$$\begin{aligned} \text{Height along } z \text{ axis: } H &= 2Nl \sin \alpha \cos(\arcsin(\tan \theta / \tan \alpha)); \\ \text{Length along } y \text{ axis: } L &= 2Ml \cos \theta; \\ \text{Thickness along } x \text{ axis: } T &= l \sin \theta. \end{aligned} \quad (4)$$

Then the projected surface area that is effective to shield sound source is $4MNl^2 \sin \alpha \cos \theta \cos(\arcsin(\tan \theta / \tan \alpha))$.

Eq. (4) indicates that with a fixed design of the constituent Miura-ori cell (with crease length l and sector α), the barrier geometry entirely depends on the folding angle θ , i.e., folding of the origami barrier remains a single DoF mechanism. Under zero-facet-thickness assumption, the origami barrier can be folded into zero height and maximum thickness $l \sin \alpha$ when $\theta \rightarrow \alpha$, and can be fully extended to a flat surface (zero thickness) with maximum height $2Nl \sin \alpha$ when $\theta \rightarrow 0^\circ$. Such excellent deployment capability comes from the reversible and single DoF foldability of Miura-ori. Hence, without replacing the product completely, the barrier geometries can be on-site reconfigured through folding to adapt different noise sources; and the deployment process requires only one actuator. Note that the flat-foldability is another extraordinary property of Miura-ori (under zero-facet-thickness assumption). Practically, the facet and crease thickness cannot be ignored, however, through certain techniques invented for thick origami [28], the Miura-ori structures can still be folded into very compact size, which could significantly improve the barriers' portability and transportability. In addition, the scale-independency of origami structures suggests that such barriers can be designed and manufactured at various length scales via different methods. For example, thin metal plates jointed with flexible hinges or coated on elastic material as layered composites are effective ways to achieve a balance between shape morphing and mechanical strength [14, 29]. To fabricate a

disposable product, hard paperboard could serve as a cheap and lightweight alternative.

2.3 Absorptive barrier

In addition to serving as a reflective sound barrier, the origami sheet can be further integrated with absorbing materials to form an absorptive assemblage. To achieve effective sound absorption, Fig. 2(c) shows a design where the folding-induced origami corrugations are exploited as sub-cavities (to provide acoustic reactance), and a micro-perforated membrane (MPM) is attached onto the front surface (to provide resistance), essentially forming a Helmholtz resonator system. The working principle of the constructed absorber is that external sound incidence causes the air molecules inside the perforations to oscillate, and the acoustic energy is dissipated through viscous effect at the small orifice boundaries [30].

Overall, the above two barrier design mechanisms (reflective and absorptive) are illustrated to show how origami concept could advance the barrier design philosophy as well as brings in numerous advantages in terms of sound isolation performance and multiple practical aspects.

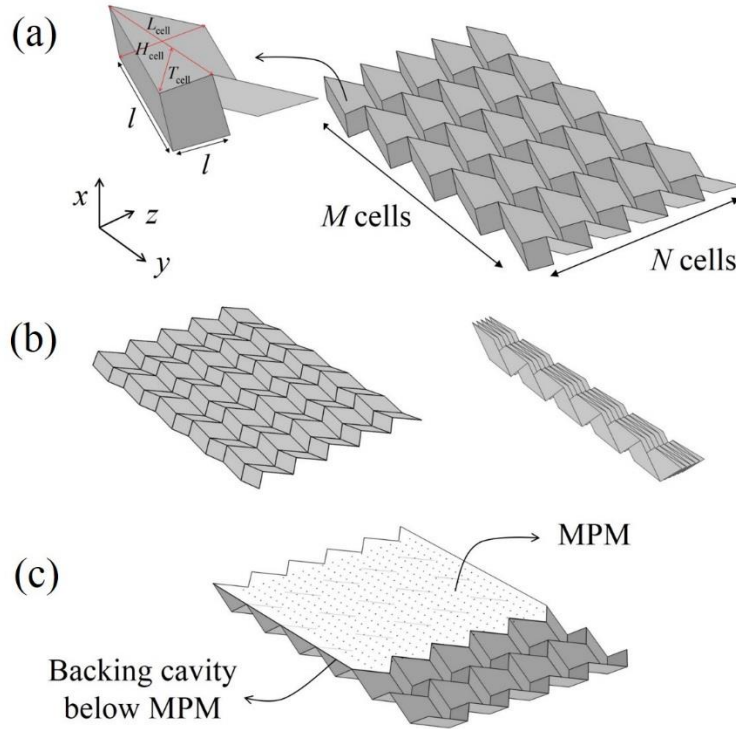


Figure 2. Conceptual designs of foldable origami barrier. (a) An $M \times N$ Miura-ori reflective barrier, with the constituent Miura-ori cell being denoted; its geometries can be significantly altered through folding. (b) Two qualitatively different configurations of the barrier. (c) An absorptive barrier comprised of a micro-perforated membrane (MPM) facing and a corrugated Miura-ori sheet, where the corrugations serve as the backing cavities.

3. Absorption analyses

The two origami barriers designed in Section 2 involves both reflection and absorption mechanisms for controlling sound. For the reflective barrier, the reflection property mainly depends on the barrier height, shape, and surface profile, which all relate to shape morphing when the origami sheet is reversibly folded. On the other hand, the absorptive barrier has two sets of design parameters, one is the orifice parameters of the MPM, and the other is the geometric parameters of the origami backing cavity.

In this section, we examine the absorption characteristics of the absorptive barrier via FE method. Experiment is also carried out to verify the FE results so that they can be employed to predict the overall performance of the origami barriers (Section 4). Particular focus of this section is put on the change of absorption frequency band with respect to the morphing of origami cavities induced by folding.

3.1 Finite element analyses

To ensure accurate numerical predictions, the acoustic characteristics should be correctly defined for the involved acoustic elements (i.e., the MPM) and boundaries (i.e., origami facets). The facets constituting the origami barrier can be considered as rigid boundaries due to its relatively large impedance over air. The MPM layer with small orifices, which is modeled as an impedance boundary in the acoustic system, is examined here in detail.

The sound absorption of micro-perforated absorber has been well studied based on thermal-viscous theory of small orifices [31]. If backed by a simple rectangular cavity, the sound absorption coefficient a can be analytically described as:

$$a = \frac{4 \operatorname{Re}(z_{\text{MPM}})}{[\operatorname{Re}(z_{\text{MPM}}) + 1]^2 + [\operatorname{Im}(z_{\text{MPM}}) - \cot(kD)]^2}, \quad (5)$$

where z_{MPM} is the complex specific impedance of the MPM, D is the depth of the backing cavity, and k is the wavenumber. The MPM impedance together with the backing cavity depth determines the frequency bands that sound can be effectively absorbed.

For the origami absorber constructed in Fig. 2(c), we establish a unit model (Fig. 3(a)) to clarify the effects of the origami cavities. The unit model is covered with a MPM, and is placed in an impedance tube with rectangular cross-section for studying the absorption coefficient (Fig. 3(b)). The absorber unit locates at the end of the tube, and a normal plane wave is excited at the entrance. Two microphones are used to separate the incident and reflected sound pressure amplitude for calculating the absorption coefficient. For simulation purpose, the acoustic impedance of a MPM is analytically described as [32]:

$$z_{\text{MPM}} = \frac{32\mu t}{\rho_0 c_0 \sigma d^2} \left[\left(1 + \frac{\kappa^2}{32} \right)^{1/2} + \frac{\sqrt{2}}{32} \kappa \frac{d}{t} \right] + \frac{j\omega t}{c_0 \sigma} \left[1 + \left(9 + \frac{\kappa^2}{2} \right)^{-1/2} + 0.85 \frac{d}{t} \right], \quad (6)$$

where μ is the air viscosity, taken as 1.8×10^{-5} Pa·s; κ is the perforation constant $\kappa = d\sqrt{\rho_0\omega/4\mu}$; ω is the angular frequency; ρ_0 and c_0 denote air density and sound speed, respectively. The MPM orifice parameters include: perforation diameter d , membrane thickness t , and perforation ratio σ .

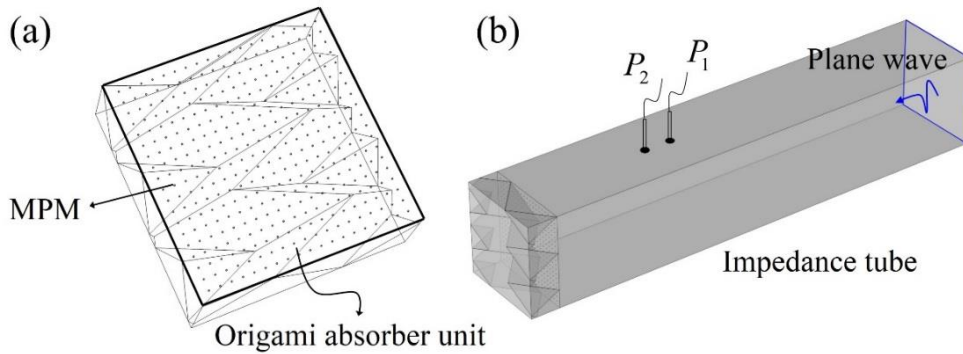


Figure 3. Schematics of (a) an origami absorber unit with MPM backed by origami cavities. The FE model for studying the absorption coefficient is illustrated in (b).

To cope with the complex geometry of the origami cavities, the commercial FE solver COMSOL is employed to solve the system response. Free-tetrahedral element

is used to discretize the computation domain, and the MPM is characterized by an interior impedance surface defined by Eq. (6). The absorption coefficient of the absorber unit can be determined using signals obtained at the two microphone locations as [33]:

$$\begin{aligned} H_{12} &= P_2 / P_1; & H_i &= e^{-jkd_{\text{mic}}}; & H_r &= e^{jkd_{\text{mic}}}; \\ r &= \frac{H_{12} - H_i}{H_r - H_{12}} e^{2jkx_1}; & a &= 1 - |r|^2. \end{aligned} \quad (7)$$

where P_1 and P_2 are the pressures picked at the two microphone; x_1 is the position of Mic 1; d_{mic} is the separation distance between two microphones; r is the reflection factor of the pressure amplitude; and a is the calculated absorption coefficient.

3.2 Prototypes and experimental tests

Prototype fabrication and experimental set-up are shown in Fig. 4. The origami cavities are 3D printed with fused deposition modelling acrylonitrile butadiene styrene (FDM ABS-P430TM) on a Stratasys FORTUS 250MC printer. The geometry of the origami cavity is $l = 0.05$ m, $\alpha = 45^\circ$, $\theta = 39.5^\circ$, and the cross-section of the sample is 0.1×0.1 m (Fig. 4(a)). The MPM for experiment is made from carbon fiber membrane of 0.5 mm in thickness, and the distributed small orifices are manufactured by Computer Numerical Control (CNC) drilling process (Fig. 4(b)). The sample is 0.1 by 0.1 m in size to fit with the cavities, and is drilled with 400 holes of diameter 0.42 mm. Hence, the MPM parameters are: $d = 0.42$ mm, $t = 0.5$ mm, and perforation ratio $\sigma = 0.65\%$. As shown in Fig. 4 (c), a straight rectangular duct of 0.6 m in length is employed for measuring the acoustic performance of the prototype. In this system, a loudspeaker installed at one end of the duct is acting as the sound source in the

measurement. The prototype is installed at the other end of the duct. Two PCB array microphones (Model 130E20), referred as ‘Mic1’ and ‘Mic2’, are used for measuring the sound pressure inside the duct, with a separation distance 20 mm. We use an NI PCI-6251 DAQ board to generate the excitation signals and to collect the response signals, with a sampling rate of 40 kHz. The sound pressures measured by the microphones are then processed based on Eq. (7) to obtain the absorption coefficient in the frequency range from 100 Hz to 1600 Hz.

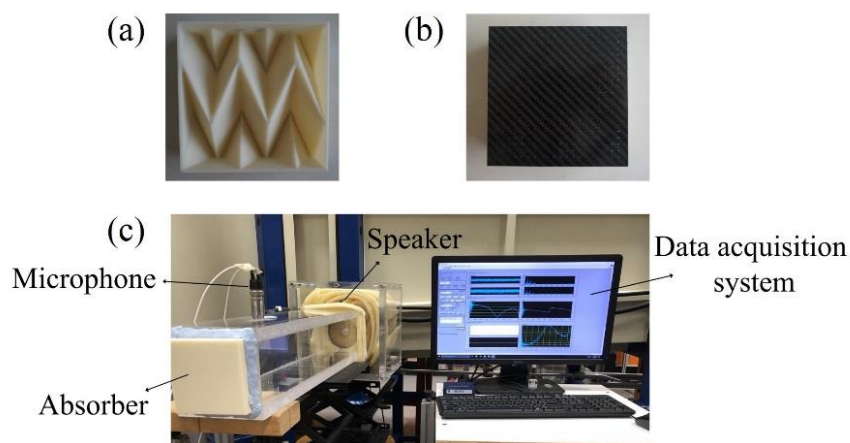


Figure 4. Experimental prototype and test setup. (a) The 3D-printed origami cavities that constitute the absorber unit. It will be covered by (b) a MPM made of carbon fiber. (c) The impedance tube with a rectangular cross-section and the acoustic measurement system.

The predicted absorption coefficient using FE method and the measured result for the absorber unit are presented in Fig. 5(a), which show very good agreement. The developed FE model is thus verified experimentally, which is reliable for IL prediction in the next section. At high frequency end, the experimental results are even better than prediction, which may be attributed to the damping effect of carbon fiber membrane. To show the effect of origami cavity on the absorption frequency band, an absorber unit comprising a simple cavity (i.e., without origami wedges) is considered and its absorption coefficient is calculated using Eq. (5). The cavity depth

of the simple cavity is set identical to the origami cavity, i.e., $D = l \sin 39.5^\circ = 0.032$ m. Figure 5(b) compares its absorption coefficient with that of the origami cavity of the same depth, but obviously the results show different absorption bands. The half-band absorption ($a > 0.5$) is from 700 Hz to 1400 Hz for the absorber unit with origami cavity, while it is from 500 Hz to 1150 Hz for the absorber unit with simple cavity. This indicates that the origami cavity with trapezoidal wedges has a significant effect on the acoustic characteristics. With identical cavity depth, the effective frequency range with origami cavity is generally higher than that with simple cavity. Furthermore, two more origami cavities with folding angles $\theta = 30^\circ$ and 20° are simulated and their absorption coefficients are included in Fig. 5(b). The general trend is that a smaller folding angle leads to a higher absorption frequency range, as a result of the reduced cavity depth. Overall, the impedance tube example here demonstrates the validity and accuracy of the FE model in predicting the characteristics of the origami absorber assembly. The model will be extended to noise barrier configuration in Section 4 to analyze the performance of the proposed origami-inspired barrier.

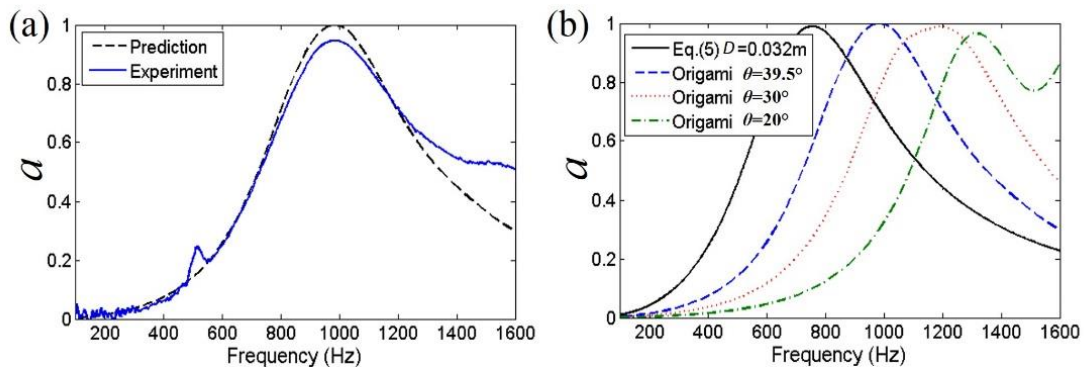


Figure 5. (a) Predicted and measured absorption coefficient for MPM absorber backed by origami cavity; (b) Absorption coefficient of absorber unit comprising simple cavity (calculated using Eq. (5)) and origami cavities with varying folding angles.

4. Barrier performance analyses

This section studies the overall performance of the designed barriers by considering both the reflection and absorption effects. Specifically, the barriers are used to shield a point source in an open acoustic space, where the IL performance is evaluated. Due to the complex geometry, FE method is adopted again, with the absorptive MPM being modeled as an acoustic impedance boundary based on Eq. (6). The validity of the numerical model has been verified in the last section.

4.1 FE model and simulation configurations

Fig. 6 shows the setup for numerical studies, where the origami barrier is modeled according to the geometric relations described in Section 2 and stands vertically in the y - z plane. Its constituent facets are taken as rigid with the structural-borne transmission through the facet being neglected. The ground surface is assumed as rigid boundary. On the barrier's left hand side (negative x -axis), a point source S is defined; a set of receiving points are defined on the other side (positive x -axis) to evaluate the sound attenuation performance. The governing equation of the prescribed acoustic domain is:

$$\nabla \cdot \left(\frac{1}{\rho_0} \nabla P \right) + \frac{\omega^2}{c_0^2} P = Q, \quad (8)$$

where P is the complex sound pressure amplitude at any point in the acoustic domain; ω is the angular frequency; and Q represents the monopole acoustic source. The MPM is modeled as an interior impedance boundary:

$$\mathbf{n} \cdot \left(\frac{1}{\rho_0} \nabla P \right) = \frac{j\omega}{Z_{\text{MPM}}} \Delta P \quad (9)$$

where \mathbf{n} is the unit vector pointing normal to the MPM surface; ΔP denotes the pressure difference on both sides of the surface; and Z_{MPM} is the effective impedance given in Eq. (6). The origami cavities formed between the MPM and origami backing sheet is also discretized and molded as individual acoustic domains, which is essentially ‘non-locally reactive’. To simulate an open space, the whole system is enclosed in a semi-sphere whose outer boundaries are defined as free-radiation surfaces.

The IL of the barrier is examined by assessing and comparing the noise mitigation performance at a given receiving point. Specifically, it is defined as the difference between the sound pressure level (SPL) in a simulation configuration without the presence of the barrier (SPL_{open}) and the SPL with the barrier ($\text{SPL}_{\text{barrier}}$), i.e. ,

$$\text{IL} = \text{SPL}_{\text{open}} - \text{SPL}_{\text{barrier}} \quad (10)$$

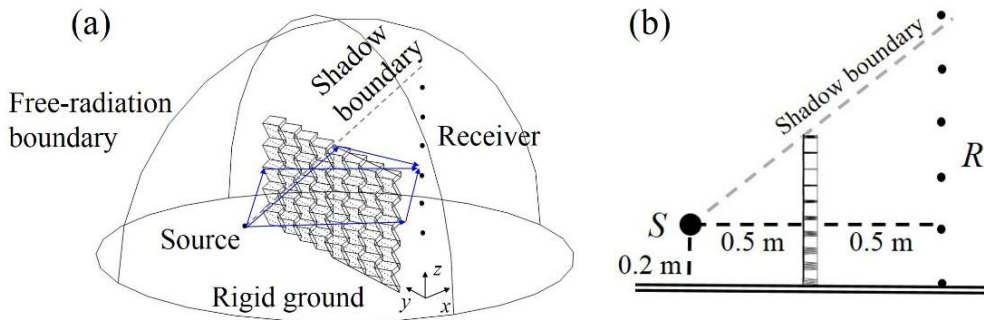


Figure 6. (a) Schematic illustration of the developed FE setup to study the insertion loss of an origami barrier. (b) Locations of the source and receivers and the shadow boundary.

Referring to Fig. 6(b), the source and receivers are assumed to locate on the center line of the barrier. The horizontal distances (along the x -axis) from the source and receiver to the barrier are set to be identical as 0.5 m. The source S is positioned

at 0.2 m above the ground, and the receivers are linearly sampled between 0 m and 1 m above the ground. Three folding angles with $\theta = 40^\circ$, 30° , and 20° are selected to show how folding would affect the IL. At these three angles, the corresponding barrier height, length and thickness are given in Table 1.

Table 1. The external geometries (height H , length L , and thickness T) and the shadow boundary height of the origami sound barrier at different folding angles.

Folding angle	Barrier height (m)	Barrier length (m)	Barrier thickness (m)	Shadow boundary height (m)
$\theta = 40^\circ$	0.385	1.23	0.064	0.57
$\theta = 30^\circ$	0.58	1.39	0.050	0.96
$\theta = 20^\circ$	0.66	1.50	0.034	1.12

Three different barriers (Fig. 7) are simulated to understand the effects of the origami sheet and the additional absorber. The Rigid Barrier (RB) is the benchmark case which is a piece of flat rigid sheet with a negligible thickness. Based on the Miura-ori cell, the Origami Rigid Barrier (ORB) is featured with a corrugated surface, whose shape depends on both the crease pattern geometries (i.e., the crease length l and the sector angle α) and the folding angle θ . Building upon the ORB, an Origami Absorptive Barrier (OAB) further incorporates the MPM to cover the origami cavities. The MPM layer is still assumed to be flat to avoid unnecessary geometric complexity and to simplify the simulations. The geometries associated with the Miura-ori unit cell are: $l = 0.1$ m, sector angle $\alpha = 45^\circ$, and the folding angle θ can vary between 0° and 45° . To form the array, 8 and 5 cells are tessellated along the y and z axes, i.e., $M = 8$ and $N = 5$. Hence, according to Eq. (4), the barrier length along the y direction is $1.6\cos\theta$ m, which can vary from 1.13 m to 1.6 m when θ changes from 45° (completely folded) to 0° (fully extended). The barrier height along the z

direction is $0.71\cos(\arcsin(\tan\theta))$, which can vary from 0 m to 0.7 m, accordingly.

For comparison purpose, the three barriers are modeled with the same corrugated edges and the same height.

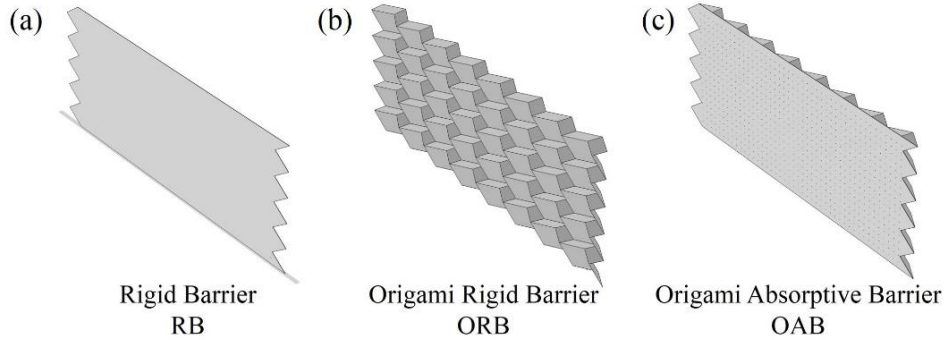


Figure 7. Three different sound barrier models: (a) rigid barrier (RB), (b) origami rigid barrier (ORB), and (c) origami absorptive barrier (OAB).

Based on the size of the barrier, a semi-sphere open space is set with a radius of 1.2 m. Free-tetrahedral element type is used to discretize the system. With a maximum allowed mesh size of 0.04 m, the total number of elements in this system is in the order of 1 million. The barrier IL is evaluated in the frequency range between 100 Hz and 2000 Hz. Further refining the element size shows no convergent issue. The computation time for each barrier case at a specific folding angle is typically about 40 hours.

To summarize, the numerical studies include three barrier configurations (RB, ORB, and OAB), each being examined at three folding angles ($\theta = 40^\circ, 30^\circ, 20^\circ$), and the IL results are evaluated at receivers between 0 m and 1 m above the ground. The obtained IL results are compared in the following subsections for analyzing the effects of folding and absorption.

4.2 Effects of folding on barrier performance

The origami barrier height and surface profile change significantly with respect to folding. As illustrated in Fig. 6, the shadow boundary is defined as the line-of-sight from the source to the barrier tip, below which the so-called shadow zone is generated [34]. Decreasing the folding angles would increase the height of the barrier and thus enlarge the shadow zone.

In Fig. 8(a)-(c), the IL spectra of rigid RB and ORB barriers at the three folding angles are displayed, with the receiver height being linearly sampled between 0 m and 1 m above the ground. The ILs of ORB are plotted in solid lines, whereas the ILs of RB are plotted in dashed lines. The IL curves between two receiver points are shifted by 10 dB so that all curves can be included in one figure for comparison. Generally, oscillatory IL behaviors are observed within the studied frequency range, with some frequencies exhibiting substantially higher IL than the others. The oscillations are caused by the complex interference effect among multiple diffraction paths from the source to the receiver, as conceptually illustrated in Fig. 6(a). Although the three IL figures show some interesting trends such as resonant-like IL rises and drops, it is still difficult to identify these resonances and define the patterns rigorously using simple geometric model. To capture such interference phenomenon, deterministic models (e.g., analytical formulations [25, 35] or FE method, which is adopted in this study) work better than geometry models based on diffraction rays. In the three figures, the ILs at the receiving points below the shadow boundary are generally higher than those above the boundary, which emphasizes the fundamental importance of blocking the

direct line-of-sight between the source and receiver. The IL at a particular receiver with a smaller folding angle (thus taller barrier) is also higher in a frequency-averaged sense.

Comparing the ILs of ORB and RB at each folding angle and each specific receiver, their very low frequency ends basically overlap with each other, while noticeable discrepancies can be observed at higher frequencies exceeding a certain frequency margin. The reason is that the acoustic wavelength has to be comparable to the length of the corrugated origami wedge so that the origami could alter the diffracted sound field. Otherwise, the barrier IL is mainly characterized by the outline of the barrier boundary. The deviation between ORB and RB could become larger at higher frequencies, or if the origami wedges are greater in size.

To show the effect of folding on the attenuation performance, the IL results are averaged with respect to frequency from 100 Hz to 2000 Hz, which generates a single mean IL at each receiver. Variations of the mean IL with respect to the three folding angles are plotted in Fig. 9. It shows that folding could significantly affect the IL results. Generally, the mean ILs with small folding angles are higher than those with large folding angles at most of the receivers. This is because higher barrier offers sound reflection over a larger area and thus the sound attenuation performance is higher. The mean IL also shows a descending trend with increasing receiver height, as diffracted sound can reach higher receivers which are located closer to the shadow boundary. Generally, receivers inside the shadow zone can maintain a mean IL of at least 5 dB in the averaged frequency range from 100 Hz to 2000 Hz.

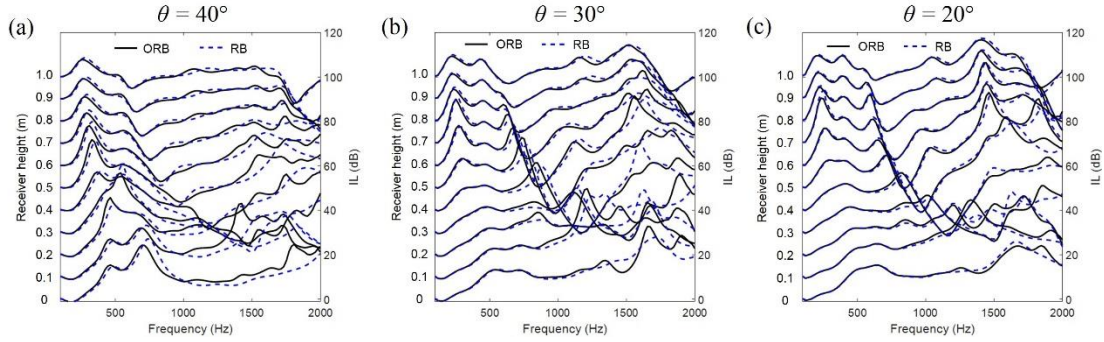


Figure 8. IL spectra of the ORB and RB at the sampled receiving points: (a) $\theta = 40^\circ$; (b) $\theta = 30^\circ$; (c) $\theta = 20^\circ$. The IL curves between two receiving points are shifted by 10 dB.

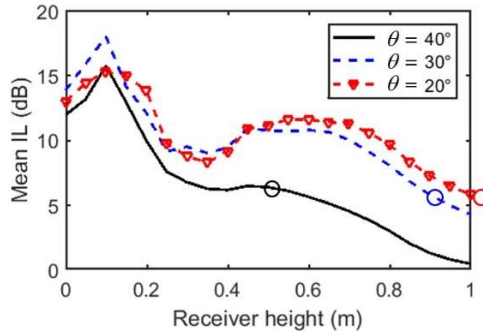


Figure 9. Frequency-averaged mean IL of the ORB at the three folding angles ($\theta = 40^\circ, 30^\circ, 20^\circ$) to show the effect of folding. The circle on each curve marks the shadow boundary, the shadow zone locates on the left side of the circle.

In sum, we show that the origami-based design endows the barrier with excellent geometric reconfigurability. The IL performance as a result of sound reflection and diffraction can be significantly tailored via folding. The IL spectra of a rigid origami barrier depend on its height, shape, and surface profile, which all relate to the initial design of origami geometry and its shape morphing, i.e., a set of variables including $\{l, \alpha, M, N, \theta\}$. Generally, by increasing the barrier height through folding, a larger

acoustic shadow zone can be obtained. By moving the receiver from bright zone to shadow zone, the IL spectrum can be remarkably raised.

4.3 Effect of absorption

The absorber unit (modeled in Fig. 3(a)) that constitutes the OAB is in principle a Helmholtz resonator system with high acoustic energy loss. To show the effect of absorption on the overall barrier performance, this section compares the performance between origami barriers with and without the MPM layers (i.e., between OAB and ORB), as well as between OAB and RB. “Extra attenuations” ΔIL are defined to examine the improvement induced by absorption. Specifically,

$$\Delta IL_1 = IL_{OAB} - IL_{ORB}, \quad \Delta IL_2 = IL_{OAB} - IL_{RB} \quad . \quad (10)$$

where IL_{OAB} , IL_{ORB} , and IL_{RB} are the insertion losses due to OAB, ORB, and RB at the same receiver, respectively.

We first examine the extra attenuation at the configurations with folding angle $\theta = 40^\circ$. Contours of ΔIL_1 with respect to receiver height (with a sampling step size of 0.05 m) and frequency are presented in Fig. 10(a). It reveals that ΔIL_1 takes positive values within the majority of the height-frequency domain, indicating that integrating MPM induces efficient sound absorption. If defining 5dB as the threshold value of substantial IL improvement, a substantial region can be determined, marked by the dashed open contour in Fig. 10(a), inside which, the benefit of MPM is significant. Note that in terms of frequency, the substantial region mainly locates from 500 Hz to 2000 Hz; in terms of receiver height, the substantial region is below 0.5m,

manifesting the importance of the shadow boundary (horizontal long-dashed line, i.e., 0.57 m for $\theta = 40^\circ$). Overall, Fig. 10(a) indicates that, to improve IL via incorporating absorption mechanism, both the absorber's effective frequency and the barrier's geometry need to be simultaneously considered.

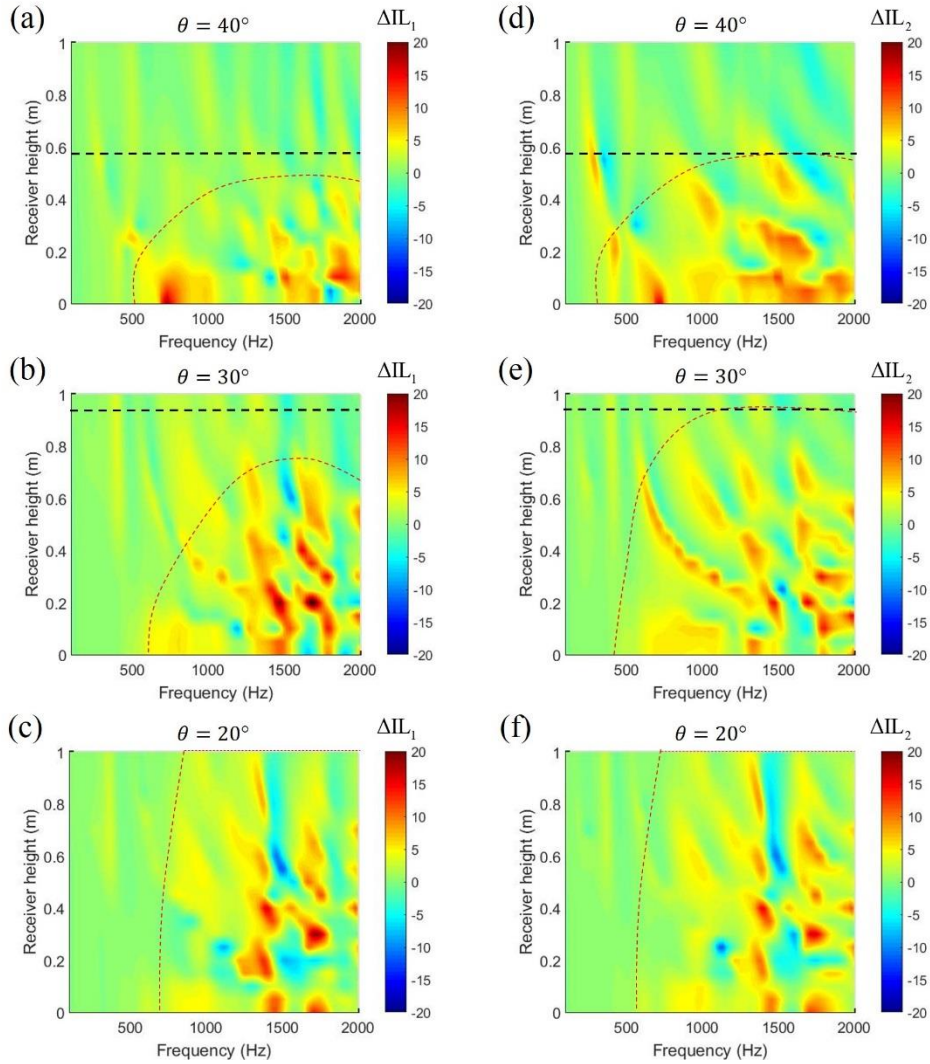


Figure 10. (a)-(c): Extra attenuation ΔIL_1 to show the improvement of OAB over ORB at the three folding angles. The horizontal dashed line marks the shadow boundary. (Note that for $\theta = 20^\circ$, the shadow boundary at 1.12 m is above the sampled receivers). The dashed open contour marks the region with substantial IL improvement. (d)-(f): Extra attenuation ΔIL_2 of OAB over RB.

In Fig. 10(b) and 10(c), ΔIL_1 at the other two folding angles $\theta = 30^\circ$ and $\theta = 20^\circ$ are presented. As the folding angle increases, the depth of the Miura-ori cavities decreases, thus shifting the substantial absorption region to higher frequencies (similar to previous analyses in Fig. 5(b)). Meanwhile, the height of the origami barrier also increases accordingly, which lifts up the shadow boundary and creates larger shadow zones. In Fig. 10(b) ($\theta = 30^\circ$), the region with substantial IL improvement encloses higher receivers up to 0.7 m, and the dominant frequencies shift higher compared to the previous case ($\theta = 40^\circ$) in Fig. 10(a). With $\theta = 20^\circ$, the substantial ΔIL_1 region is further raised to 1 m as observed from Fig. 10(c).

To show the effects of both absorption and origami geometry, the improvement of OAB over flat RB (i.e., ΔIL_2) are displayed in Fig. 10(d)-(f). Basically, the effective regions with positive ΔIL_2 are in the same frequency range as the previous comparison between OAB and ORB (i.e., ΔIL_1), and are also constrained by the shadow boundary. However, the zones with substantial absorption are extended to higher receivers as shown in the cases with $\theta = 40^\circ$ and 30° , which are closer to the shadow boundary. Because ΔIL_1 is only attributed to the added absorption while ΔIL_2 includes both origami and absorption effects, better ΔIL_2 over larger receiving area could mean combining origami and absorption together provides extra benefit.

In sum, the major factors affecting the performance of the proposed origami barrier (with fixed source and receiver location) are summarized as follows: (i) the height and length of the barrier, which determine the diffracted sound paths. They are

functions of origami geometry and folding angle, i.e., $\{l, \alpha, M, N, \theta\}$; (ii) the barrier surface profile of the corrugated wedges; and (iii) the absorptive facing covering the origami cavities. For MPM, a set of parameters $\{d, t, \sigma\}$ are included and the resonant working frequency is related to the origami thickness determined by l and θ . Note that the three factors are closely related to the folding-induced geometry changes.

4.4 Discussion on rich origami design

It is worth mentioning that although this study is developed based on a specific type of origami cell, Miura-ori, the vast origami library can enable other designs with particular geometric features that are acoustically beneficial. For example, Figure 11 demonstrates another Miura-ori based barrier design, whose crease patterns are tailored in order to form a barrier with curved top. The barrier can be deployed into the designed shape, extended to a flat surface, and folded to zero-width upon a single DoF folding mechanism. The angle and length of the curved top, which exert significant effect on the resulting acoustic shadow zone and thus the attenuation performance, can be designed and customized based on the origami knowledge.

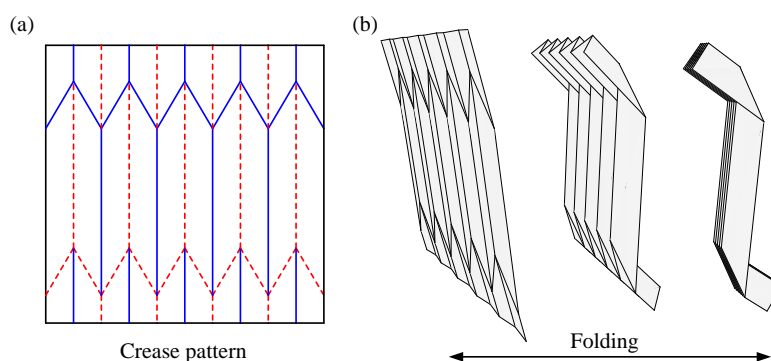


Figure 11. A Miura-ori based barrier design with tailored crease pattern to (a) form curved top (b) via folding. In the crease pattern, the solid and dashed lines denote the mountain and valley creases, respectively.

4. Summary and conclusions

The new ideas explored in this paper aim at providing a design platform based on which the long-standing challenges of sound barriers may be overcome. These challenges include the bulky barrier size, the lack of geometric and acoustic tunability with respect to different noise sources, the low portability and cumbersome assembling/disassembling processes. The origami technique offers an unconventional solution to these challenges by exploiting the excellent foldability and folding-induced geometry changes. By the same token, origami-induced geometrical changes bring along an alternation in the acoustic characteristics of the sound barriers, in terms of both reflective and absorptive effects. At this stage, although only conceptual designs have been proposed, the uncovered fundamental mechanisms well demonstrate the capability and advantages of origami in advancing the state of the art of sound barrier technology.

Specifically, in this study, Miura-ori cells are employed as the constituent units of the origami barriers, which are then used to shield a point source in an acoustic free-space. In addition to serving as a reflective barrier (i.e., ORB), the folding induced corrugated cavities are further integrated with MPM to form absorbers such that the barrier is endowed with absorptive capability (i.e., OAB). Through FE analyses, performances of the ORB and OAB are compared with that of a simple flat RB to show the merits of origami folding and absorptive MPM on the IL performance. Note that in order to get an accurate estimation, the OAB element were studied both numerically and experimentally using the impedance tube. The agreement between

numerical and experimental results ensures the applicability of the established FE model in predicting the overall performance of the OAB.

The obtained results indicate that the origami barrier significantly affect the IL performance. The corresponding IL response in the frequency domain is a result of the complex interference phenomenon due to the diffracted sound waves from the three-dimensional barrier edges. The proposed origami barrier has two mechanisms: sound reflection/diffraction and sound absorption based on MPM. Origami offers tunability to enrich both mechanisms: folding actively changes the acoustic shadow zone and the barrier's surface profile; the absorbing OAB built upon ORB and MPM allows IL improvement in desired frequencies.

Finally, it is worth mentioning that the proposed origami concepts for noise barrier design are versatile and can be extended or transferred into other forms. Such origami-inspired barriers could provide enhanced sound attenuation that are comparable to or exceed that of conventional barriers, and meanwhile offer practical advantages in terms of simplicity, portability, reconfigurability, and low-cost. Beyond demonstrating the high potentials and the promising prospects, our ongoing efforts seek to propose other innovative origami designs that could possess more acoustically beneficial characteristics, and to explore effective tools (either analytical, numerical, or semi-analytical) for predicting the acoustic performance and optimizing the origami designs.

References

- [1] C. Yang, J. Pan, L. Cheng, A mechanism study of sound wave-trapping barriers, *The Journal of the Acoustical Society of America*, 134 (3) (2013) 1960-1969.
- [2] P. Menounou, E.S. Papaefthymiou, Shadowing of directional noise sources by finite noise barriers, *Applied Acoustics*, 71 (4) (2010) 351-367.
- [3] M.R. Monazzam, Y.W. Lam, Performance of profiled single noise barriers covered with quadratic residue diffusers, *Applied Acoustics*, 66 (6) (2005) 709-730.
- [4] B.-J. Jin, H.-S. Kim, H.-J. Kang, J.-S. Kim, Sound diffraction by a partially inclined noise barrier, *Applied Acoustics*, 62 (9) (2001) 1107-1121.
- [5] F.J. Fahy, D.G. Ramble, J.G. Walker, M. Sugiura, Development of a novel modular form of sound absorbent facing for traffic noise barriers, *Applied Acoustics*, 44 (1) (1995) 39-51.
- [6] J. Kook, K. Koo, J. Hyun, J.S. Jensen, S. Wang, Acoustical topology optimization for Zwicker's loudness model – Application to noise barriers, *Computer Methods in Applied Mechanics and Engineering*, 237-240 (2012) 130-151.
- [7] F. Asdrubali, G. Pispola, Properties of transparent sound-absorbing panels for use in noise barriers, *The Journal of the Acoustical Society of America*, 121 (1) (2007) 214-221.
- [8] K.H. Kim, G.H. Yoon, Optimal rigid and porous material distributions for noise barrier by acoustic topology optimization, *Journal of Sound and Vibration*, 339 (2015) 123-142.
- [9] N. Han, X. Qiu, A study of sound intensity control for active noise barriers,

Applied Acoustics, 68 (10) (2007) 1297-1306.

[10] F. Koussa, J. Defrance, P. Jean, P. Blanc-Benon, Acoustical Efficiency of a Sonic Crystal Assisted Noise Barrier, *Acta Acustica united with Acustica*, 99 (3) (2013) 399-409.

[11] T. Ishizuka, K. Fujiwara, Performance of noise barriers with various edge shapes and acoustical conditions, *Applied Acoustics*, 65 (2) (2004) 125-141.

[12] W. Ho, W. Wylog, N. Yasir, Lightweight noise barrier, *Inter-Noise 2014*, Melbourne, Australia (2014).

[13] A.E.D. Grosso, P. Basso, Adaptive building skin structures, *Smart Materials and Structures*, 19 (12) (2010) 124011.

[14] E.T. Filipov, T. Tachi, G.H. Paulino, Origami tubes assembled into stiff, yet reconfigurable structures and metamaterials, *Proceedings of the National Academy of Sciences*, 112 (40) (2015) 12321-12326.

[15] S. Felton, M. Tolley, E. Demaine, D. Rus, R. Wood, A method for building self-folding machines, *Science*, 345 (6197) (2014) 644-646.

[16] J.L. Silverberg, A.A. Evans, L. McLeod, R.C. Hayward, T. Hull, C.D. Santangelo, I. Cohen, Using origami design principles to fold reprogrammable mechanical metamaterials, *Science*, 345 (6197) (2014) 647-650.

[17] F. Hongbin, Z. Yetong, K.W. Wang, Origami-based earthworm-like locomotion robots, *Bioinspiration & Biomimetics*, 12 (6) (2017) 065003.

[18] D.T. Lynd, R.L. Harne, Strategies to predict radiated sound fields from foldable, Miura-ori-based transducers for acoustic beamfolding, *The Journal of the Acoustical*

Society of America, 141 (1) (2017) 480-489.

[19] C. Zou, D.T. Lynd, R.L. Harne, Acoustic Wave Guiding by Reconfigurable Tessellated Arrays, *Physical Review Applied*, 9 (1) (2018) 014009.

[20] S. Babae, J.T.B. Overvelde, E.R. Chen, V. Tournat, K. Bertoldi, Reconfigurable origami-inspired acoustic waveguides, *Science Advances*, 2 (11) (2016).

[21] M. Thota, K.W. Wang, Reconfigurable origami sonic barriers with tunable bandgaps for traffic noise mitigation, *Journal of Applied Physics*, 122 (15) (2017) 154901.

[22] M. Thota, S. Li, K.W. Wang, Lattice reconfiguration and phononic band-gap adaptation via origami folding, *Physical Review B*, 95 (6) (2017) 064307.

[23] K.M. Li, H.Y. Wong, A review of commonly used analytical and empirical formulae for predicting sound diffracted by a thin screen, *Applied Acoustics*, 66 (1) (2005) 45-76.

[24] Z. Maekawa, Noise reduction by screens, *Applied Acoustics*, 1 (3) (1968) 157-173.

[25] T. Terai, On calculation of sound fields around three dimensional objects by integral equation methods, *Journal of Sound and Vibration*, 69 (1) (1980) 71-100.

[26] S.M.B. Fard, H. Peters, N. Kessissoglou, S. Marburg, Three-dimensional analysis of a noise barrier using a quasi-periodic boundary element method, *The Journal of the Acoustical Society of America*, 137 (6) (2015) 3107-3114.

[27] M. Schenk, S.D. Guest, Geometry of Miura-folded metamaterials, *Proceedings of the National Academy of Sciences*, 110 (9) (2013) 3276-3281.

- [28] Y. Chen, R. Peng, Z. You, Origami of thick panels, *Science*, 349 (6246) (2015) 396-400.
- [29] H. Fang, S. Li, H. Ji, K.W. Wang, Dynamics of a bistable Miura-origami structure, *Physical Review E*, 95 (5) (2017) 052211.
- [30] X. Yu, L. Cheng, J.-L. Guyader, Modeling vibroacoustic systems involving cascade open cavities and micro-perforated panels, *The Journal of the Acoustical Society of America*, 136 (2) (2014) 659-670.
- [31] D.-Y. Maa, Potential of microperforated panel absorber, *The Journal of the Acoustical Society of America*, 104 (5) (1998) 2861-2866.
- [32] X. Yu, L. Cheng, X. You, Hybrid silencers with micro-perforated panels and internal partitions, *The Journal of the Acoustical Society of America*, 137 (2) (2015) 951-962.
- [33] J.Y. Chung, D.A. Blaser, Transfer function method of measuring in-duct acoustic properties. I. Theory, *The Journal of the Acoustical Society of America*, 68 (3) (1980) 907-913.
- [34] D.C. Hothersall, S.N. Chandler-Wilde, M.N. Hajmirzae, Efficiency of single noise barriers, *Journal of Sound and Vibration*, 146 (2) (1991) 303-322.
- [35] Y.W. Lam, S.C. Roberts, A simple method for accurate prediction of finite barrier insertion loss, *The Journal of the Acoustical Society of America*, 93 (3) (1993) 1445-1452.

Figure captions

Figure 1. Geometry of a Miura-ori cell at the (a) flat state and a (b) partly folded state. The internal solid and dashed lines denote the “mountain” and “valley” creases, respectively.

Figure 2. Conceptual designs of foldable origami barrier. (a) An $M \times N$ Miura-ori reflective barrier, with the constituent Miura-ori cell being denoted; its geometries can be significantly altered through folding. (b) Two qualitatively different configurations of the barrier. (c) An absorptive barrier comprised of a micro-perforated membrane (MPM) facing and a corrugated Miura-ori sheet, where the corrugations serve as the backing cavities.

Figure 3. Schematics of (a) an origami absorber unit with MPM backed by origami cavities. The FE model for studying the absorption coefficient is illustrated in (b).

Figure 4. Experimental prototype and test setup. (a) The 3D-printed origami cavities that constituent the absorber unit. It will be covered by (b) a MPM made of carbon fiber. (c) The impedance tube with a rectangular cross-section and the acoustic measurement system.

Figure 5. (a) Predicted and measured absorption coefficient for MPM absorber backed by origami cavity; (b) Absorption coefficient of absorber unit comprising simple cavity (calculated using Eq. (5)) and origami cavities with varying folding angles.

Figure 6. (a) Schematic illustration of the developed FE setup to study the insertion loss of an origami barrier. (b) Locations of the source and receivers and the shadow boundary.

Figure 7. Three different sound barrier models: (a) rigid barrier (RB), (b) origami rigid barrier (ORB), and (c) origami absorptive barrier (OAB).

Figure 8. IL spectra of the ORB and RB at the sampled receiving points: (a) $\theta = 40^\circ$; (b) $\theta = 30^\circ$; (c) $\theta = 20^\circ$. The IL curves between two receiving points are shifted by 10 dB.

Figure 9. Frequency-averaged mean IL of the ORB at the three folding angles ($\theta = 40^\circ, 30^\circ, 20^\circ$) to show the effect of folding. The circle on each curve marks the shadow boundary, the shadow zone locates on the left side of the circle.

Figure 10. (a)-(c): Extra attenuation ΔIL_1 to show the improvement of OAB over ORB at the three folding angles. The horizontal dashed line marks the shadow boundary. (Note that for $\theta = 20^\circ$, the shadow boundary at 1.12 m is above the sampled receivers). The dashed open contour marks the region with substantial IL improvement. (d)-(f): Extra attenuation ΔIL_2 of OAB over RB.

Figure 11. A Miura-ori based barrier design with tailored crease pattern to (a) form curved top (b) via folding. In the crease pattern, the solid and dashed lines denote the mountain and valley creases, respectively.

Table caption

Table 1. The external geometries (height H , length L , and thickness T) and the shadow boundary height of the origami sound barrier at different folding angles.